Available online at www.sciencedirect.com
ScienceDirect
Journal of Sound and Vibration 302 (2007) 821–840
JOURNAL OF SOUND AND VIBRATION
www.elsevier.com/locate/jsvi

Helicopter rotor-fuselage aeroelasticity modeling and solution using the partition-iteration method

J.J. Xiong*, X. Yu

Aircraft Department, Beihang University, Beijing 100083, People's Republic of China

Received 26 February 2006; received in revised form 27 November 2006; accepted 6 December 2006
Available online 5 February 2007

Abstract

This paper seeks to outline a novel coupled helicopter rotor-fuselage model and a new partition-iteration solution philosophy to predict structural response and rotor blade vibration loads. Based on a two-dimensional quasi-steady aerodynamics model, non-inertial coordinates and beam element with five nodes and 15 degrees of freedom (dofs) are first used to establish the aeroelastic differential equations of rotor blade vibration motion to describe exactly various inhomogeneities of the rotor blade including the longitudinal variation of its axial force. Three rigid body freedoms are subsequently allowed at the root of the rotor blade to describe the different hub connections, through which, the mixed truss girder-beam model of the fuselage structure is combined with the aeroelastic model of the rotor blade and the helicopter coupled rotor-fuselage model is established. The new partition-iteration solving philosophy is developed to allow solution of the periodic response of the nonlinear coupled multi-freedom dynamic system. Finally, the new model and its solution were used to compute some vibration loads of a helicopter model, and the obtained results have a good agreement with those of previous works.

1. Introduction

As is well known, the highly complex and unsteady aerodynamic loads on helicopter blades cause significant elastic blade vibration motions, which, in turn, changes the aerodynamic and structural loading along the blade. Thus, the analysis of helicopter vibration and blade loads taking into account the aero-elastic interaction has become a fascinating problem and a challenge in rotorcraft research, and the topic has been received much attention for several decades [1,2]. To investigate the vibration problem of helicopter blades, the rotating beams were first used to model helicopter blades through adequate and necessary simplification and approximation. In general, the engineering beam theory is used in determining the approximate free vibration response [3–7]. Friedmann and Straub [8] formulated, linearized and discretized the equations of blade motion using a local Galerkin method of weighted residuals to result in a finite element formulation of the aeroelastic problem based on a finite-element method of variable order. Sivaneri and Chopra [9], Thakkar

*Corresponding author.
E-mail address: jjxiong@buaa.edu.cn (J.J. Xiong).

0022-460X/$ - see front matter © 2007 Elsevier Ltd. All rights reserved.
doi:10.1016/j.jsv.2006.12.009

Nomenclature

$[C_F]$	damp matrix of fuselage
E	Young's modulus
$\{f_{HF}(t)\}$	force vector on hub of fuselage
$\{f_F(t)\}$	other force vector on fuselage
$[K_F]$	stiffness matrix of fuselage
$[M_F]$	mass matrix of fuselage
R_0	inertial coordinate system of $O_{h0}X_{h0}Y_{h0}Z_{h0}$ with the origin fixed at the center of the hub
R_1	coordinate system of $O_hX_hY_hZ_h$, the inertial coordinates system R_0 rotated by an angle of ω_t around the axis of Z_{h0}
R_2	coordinate system of $O_fX_fY_fZ_f$, the coordinates system R_1 rotated by an angle of $(\beta_0+\beta)$ around the axis of Y_h with the origin fixed at the flap hinge
R_3	coordinate system of $O_lX_lY_lZ_l$, the coordinates system R_2 rotated by an angle of ξ around the axis of Z_f with the origin fixed at the lag hinge
R_4	coordinate system of $O_fX_fY_fZ_p$, the coordinates system R_3 rotated by an angle of θ_p around the axis of X_l with the origin fixed at the variable-pitch hinge
R_5	coordinate system of $O_sX_sY_sZ_s$, the coordinates system R_4 rotated by an angle of ξ_0 around the axis of Z_l with the origin fixed at the sweepback hinge
R_6	coordinate system of $P_0X\eta\xi$ without flexure
R_7	coordinate system of $P_0'X'\eta'\xi'$ with flexure
S	Gauss integral coordinates with an interval of $[-1,1]$
T_{ij}	coordinate transformation matrix
u	axial displacement
v	lag displacement
w	flap displacement
μ	Poisson's ratio
θ	pre-torsion angle
ϕ	elastic torsion angle
Ω	angular velocity

and Ganguli [10] implemented Hamilton's principle as a variational principle to obtain a finite-element representation for the analysis of rotor blade. Bauchau and Hong [11] applied the finite-element method in time to analyze response and stability of beams undergoing large deflections and rotations, basing their work on Floquet's theory. Celi and Friedmann [12,13] described, respectively, the methods to formulate the aeroelastic stability and response problem for helicopter rotor blades, using an implicit aerodynamic and structural formulation based on a combination of a finite-element model of blade and a quasilinearization solution technique. Crespo Da Silva [14] established a nonlinear partial differential equations of rotor blade vibration motion by taking into account the geometrical nonlinearities and analyzed the dynamic stability of vibration motion. In order to reduce vibration load at the rotor hub causing helicopter vibration, Ganguli and El-Sinawi et al. [15–17] used a rotating flexible beam to model the rotor blade for an aeroelastic analysis based on finite elements and the optimum approaches for rotor blade design were investigated and discussed.

However, in above aeroelastic analysis of helicopter rotor blade [3–17], the influence of fuselage on vibration motion of rotor blade has not been taken into account. In reality, fuselage motion is known to have an influence on hub loads [18,19]. Coupled rotor-fuselage models are therefore needed to investigate the rotor-fuselage interaction and many researchers have proposed various methods. Rutkowski [20] investigated the effect of rotor/fuselage coupling on vibration predictions using a simplified structural model of a helicopter in hover according to a two degree-of-freedom (dof) beam finite element. Hsu and Peter [21] developed a new impedance-matching method by the matching of rotor and fuselage impedances for coupled rotor/fuselage vibration analysis. Kunz [22] implemented the impedance-matching method to solve the equations of motion for a uniform elastic blade, the hub-load equations and the fuselage equations of motion for a fully coupled rotor-fuselage vibration model to obtain the blade and fuselage responses, as well as the hub loads. Stephens and Peter [23] presented an iterative method and a fully coupled method to analyze the response of a rotor-body system. Cribbs et al. [24] derived a set of dynamic equations of motion for a rotor-fuselage system and the solution was obtained by using the harmonic balance technique. Bauchau et al. [25] used a floating frame approach to formulate the coupled rotor-fuselage system with finite motions and analyzed the response by means of the component mode synthesis method.

It is interesting to note in the above reviews that a large number of researches are grouped according to some important issues such as rotor blade vibration, coupled rotor/fuselage vibration and solving the coupled differential equations of rotor-fuselage motion. There is however lack of knowledge about the integral coupled rotor/fuselage vibration model in hover and forward flight by means of a nonlinear flexible multi-body, multi-freedom dynamic representation based on the finite-element method and the partition-iteration method to yield a direct solution of the nonlinear coupled differential equations, which is the focus of this paper.

2. The rotor blade differential equations of vibration motion and their solutions

2.1. The coordinate system

The coordinate systems adopted for the fuselage and blade model are shown in Figs. (1–3). The equations of motion for the rotor blade and fuselage are formulated in the coordinate systems of R_1 and R_0, respectively. The transformation matrix between R_1 and R_0 is

$$[T_{10}] = \begin{bmatrix} \cos\omega t & \sin\omega t & 0 \\ -\sin\omega t & \cos\omega t & 0 \\ 0 & 0 & 1 \end{bmatrix}. \tag{1}$$

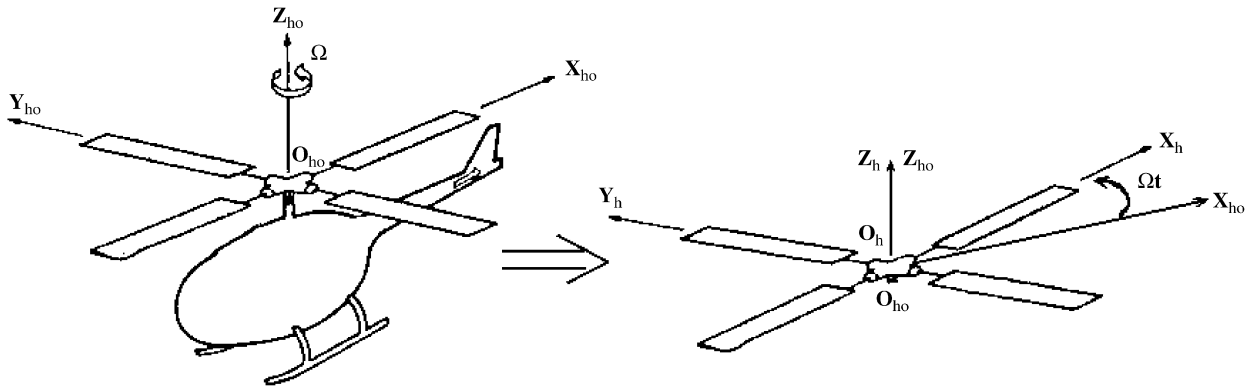

Fig. 1. Coordinate system for helicopter modeling.

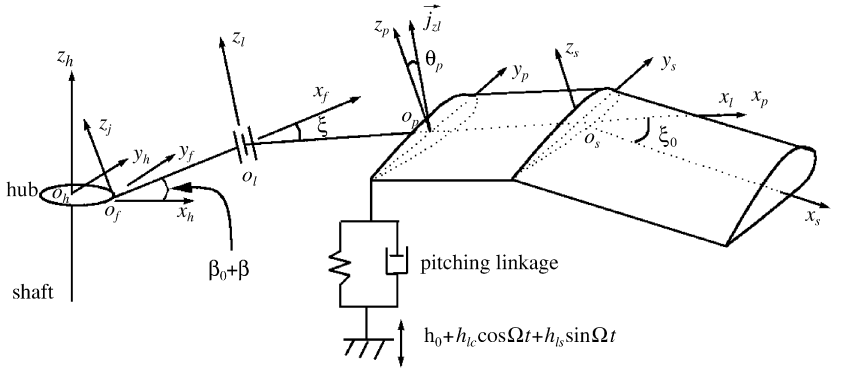

Fig. 2. Coordinate system for blade modeling.

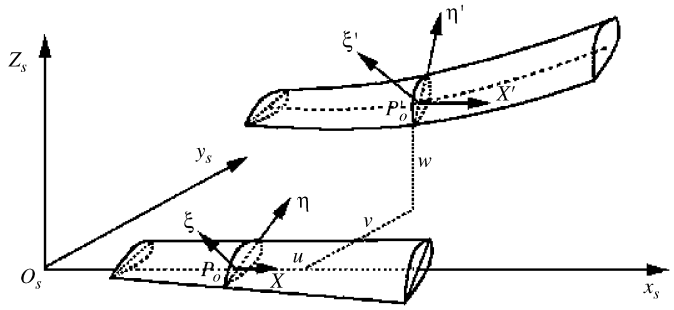

Fig. 3. Coordinate system for beam element of rotor blade with and without flexion.

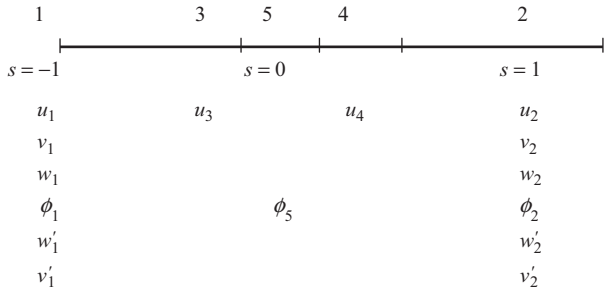

Fig. 4. Degrees-of-freedom and nodes of beam element of rotor blade.

2.2. Element and interpolating function

In order to describe the quadratic variation of the centrifugal inertial force in the axial direction, the cubic interpolating function is adopted for the axial displacement, which results in an axial strain with a quadratic variation. Four axial displacement nodes are allocated, one at each of the two ends and two interior nodes within the element. A similar quadratic axial variation also appears in the angle of torsion, with three torsion nodes being allocated, one at each end and one at the center of the element. In addition, the cubic interpolating function is adopted for the transverse flexural displacement of v and w. Consequently, the beam element has 15 dofs and five nodes (shown in Fig. 4) [10,13]. From Fig. 4, it is observed that nodes 1 and 2 have six dofs each. Nodes 3 and 4 have only one axial displacement freedom, and node 5 has one torsional freedom. The interpolating expressions of u, v, w and ϕ are listed, respectively, in Appendix A.

2.3. Elastic potential energy

The fundamental assumptions are made for the analysis as follows [10]:

(i) Mid-line of a plate segment does not deform in its own plane, or the in-plane warping of the cross-section is neglected;
(ii) the normal stress in the contour direction, $\sigma_{\eta\eta}$ is neglected relative to the normal axial stress σ_{xx}; and
(iii) rotor blade is a long slender beam and hence the uniaxial stress assumptions can be made; $\sigma_{\eta\eta} = \sigma_{\zeta\zeta} = \tau_{\eta\zeta} = 0$.

According to the theory of beams with small strain and moderately large deflection [10,13] and nonlinear continuum mechanics [26], the Green's strain tensor in curvilinear coordinates of R_6 can be derived as

$$\begin{aligned}\varepsilon_{xx} &= u' + \frac{1}{2}\left(v'^2 + w'^2\right) + v''[\xi\sin(\theta+\phi) - \eta\cos(\theta+\phi)] \\ &\quad - w''[\eta\sin(\theta+\phi) + \xi\cos(\theta+\phi)] + \left(\theta'\phi' + \frac{1}{2}\phi'^2\right)(\eta^2+\xi^2), \\ \varepsilon_{x\eta} &= -\frac{1}{2}\phi'\xi = \varepsilon_{\eta x}, \\ \varepsilon_{x\xi} &= \frac{1}{2}\phi'\eta = \varepsilon_{\xi x}. \end{aligned} \tag{2}$$

The variational formulations of the elastic strain energy density and elastic strain energy can be obtained as

$$\delta e = \begin{bmatrix}\varepsilon_{xx} & \varepsilon_{x\eta} & \varepsilon_{x\xi}\end{bmatrix}\bar{A}\begin{bmatrix}\delta\varepsilon_{xx} & \delta\varepsilon_{x\eta} & \delta\varepsilon_{\xi x}\end{bmatrix}^{\mathrm{T}}. \tag{3}$$

From Eq. (3), the variational formulation of elastic strain energy is then obtained as

$$\delta U = \iint_A \delta e\delta A = \bar{V}_x(\delta u' + v'\delta v' + w'\delta w') + \bar{M}_z(\delta v'' + w''\delta\phi). \tag{4}$$

Transformation of Eq. (4) gives

$$\delta U = \iint_A \delta e\delta A\delta = -\bar{M}_y(\delta w'' - v''\delta\phi) + GJ\phi'\delta\phi, \tag{5}$$

where $\bar{A}$, $\bar{V}_x$, $\bar{M}_y$, $\bar{M}_z$ and J are the section properties and defined in Appendix B.

Furthermore, one has

$$\int_l \mathrm{d}x \iint_A \delta e\,\mathrm{d}A = \sum_{i=1}^{15} Q_i^{E_e}\delta q_i, \tag{6}$$

where the superscript E_e represents elastic potential energy, and $Q_i^{E_e}$ represents the generalized elastic force corresponding to the nodal freedom of $(q_1, q_2, ..., q_{15})$. Thus, the tangential elastic matrix can be obtained through the differentiation of $Q_i^{E_e}$ with respect to the nodal coordinate:

$$K_{ij}^{E_e} = \frac{\partial Q_i^{E_e}}{\partial q_j} = \frac{\partial}{\partial q_i\partial q_j}\int_l \mathrm{d}x \iint_A \delta e\,\mathrm{d}A = K_{ji}^{E_e} \quad (i,j = 1,2,3,\ldots,15). \tag{7}$$

2.4. Kinetic energy

At an arbitrary point $P(x,\eta,\xi)$ on the blade with a sweepback deformation, the radius vector from the hub is

$$\begin{aligned}\vec{r}_p &= b_0\vec{i}_{xh} + d_0\vec{i}_{xf} + a_0\vec{i}_{xl} + s_0\vec{i}_{xp} + (x+u,v,w)\left[\vec{i}_{xs},\vec{i}_{ys},\vec{i}_{zs}\right]^{\mathrm{T}} + (o,\eta,\xi)\left[\vec{i}_{x'},\vec{i}_{\eta'},\vec{i}_{\xi'}\right]^{\mathrm{T}} \\ &= \left(x_p,y_p,z_p\right)\left[\vec{i}_{xh},\vec{i}_{yh},\vec{i}_{zh}\right]^{\mathrm{T}}\end{aligned} \tag{8}$$

with

$$\begin{aligned}(x_{po},y_{po},z_{po}) &= (b_0,0,0) + (d_0,0,0)T_{21} + (a_0,0,0)T_{32}T_{21} + (s_0,0,0)T_{43}T_{32}T_{21} + (x+u,v,w)T_{54}T_{43}T_{32}T_{21}, \\ \left(x_{p\eta},y_{p\eta},z_{p\eta}\right) &= (0,1,0)T_{75}T_{54}T_{43}T_{32}T_{21}, \\ \left(x_{p\xi},y_{p\xi},z_{p\xi}\right) &= (0,0,1)T_{75}T_{54}T_{43}T_{32}T_{21},\end{aligned}$$

where T_{ij} $(i = 1, 2, \ldots, 7; j = 1, 2, \ldots, 4)$ are coordinate transformation matrixes and are defined in Appendix C.

It is therefore possible to obtain the kinetic energy of an element of beam with the mass $\rho \mathrm{d}V$ at the point P:

$$\mathrm{d}T = \frac{1}{2}\rho\,\mathrm{d}V\left(\dot{x}_p^2 + \dot{y}_p^2 + \dot{z}_p^2\right). \tag{9}$$

The variation of the kinetic energy is

$$\delta T = \delta \iiint_V \mathrm{d}T = -\int_l \mathrm{d}x \iint_A \rho\,\mathrm{d}S(\bar{Q}_i^{T_x} + \bar{Q}_i^{T_y} + \bar{Q}_i^{T_Z})\delta q_i^e, \tag{10}$$

where the superscript T represents kinetic energy and is listed in Appendix D.

In order to evaluate the contributions of $\bar{Q}_i^{T_x}$ in the linearized equation, substituting $q_i^e + \Delta q_i^e$, $\dot{q}_i^e + \Delta\dot{q}_i^e$ and $\ddot{q}_i^e + \Delta\ddot{q}_i^e$ into q_i^e, $\dot{q}_i^e$ and $\ddot{q}_i^e$ in formulation of $\bar{Q}_i^{T_x}$, respectively, and expanding the formulation into Taylor's series give

$$\begin{aligned}\bar{Q}_i^{T_x}(q_i^e + \Delta q_i^e, \dot{q}_i^e + \Delta\dot{q}_i^e, \ddot{q}_i^e + \Delta\ddot{q}_i^e) = {} & \ddot{x}_p\frac{\partial x_p}{\partial q_i^e} + \left(\frac{\partial x_p}{\partial q_i^e}\frac{\partial x_p}{\partial q_j^e}\right)\Delta\ddot{q}_j^e + \left(2\frac{\partial x_p}{\partial q_i^e}\frac{\partial \dot{x}_p}{\partial q_j^e}\right)\Delta\dot{q}_j^e \\ & \text{(I)} \qquad \text{(II)} \qquad \text{(III)} \\ & + \left(\frac{\partial x_p}{\partial q_i^e}\frac{\partial \ddot{x}_p}{\partial q_j^e} + \ddot{x}_p\frac{\partial^2 x_p}{\partial q_i^e \partial q_j^e}\right)\Delta q_j^e + o(\Delta^2). \\ & \text{(IV)}\end{aligned} \tag{11}$$

The items (I), (II), (III) and (IV) in Eq. (11) yield the contributions of kinetic energy involving: the element node force vector, element tangential mass matrix, damping matrix and stiffness matrix:

$$Q_i^{T_e} = \int_l \mathrm{d}x \iint_A \mathrm{d}A\left(\ddot{x}_p\frac{\partial x_p}{\partial q_i^e} + \ddot{y}_p\frac{\partial y_p}{\partial q_i^e} + \ddot{z}_p\frac{\partial z_p}{\partial q_i^e}\right), \tag{12}$$

$$M_{ij}^{T_e} = \int_l \mathrm{d}x \iint_A \mathrm{d}A\left(\frac{\partial x_p}{\partial q_i^e}\frac{\partial x_p}{\partial q_j^e} + \frac{\partial y_p}{\partial q_i^e}\frac{\partial y_p}{\partial q_j^e} + \frac{\partial z_p}{\partial q_i^e}\frac{\partial z_p}{\partial q_j^e}\right), \tag{13}$$

$$C_{ij}^{T_e} = \int_l \mathrm{d}x \iint_A \mathrm{d}A\,2\left(\frac{\partial \dot{x}_p}{\partial q_i^e}\frac{\partial x_p}{\partial q_j^e} + \frac{\partial y_p}{\partial q_i^e}\frac{\partial \dot{y}_p}{\partial q_j^e} + \frac{\partial z_p}{\partial q_i^e}\frac{\partial \dot{z}_p}{\partial q_j^e}\right), \tag{14}$$

$$\begin{aligned}K_{ij}^{T_e} = {} & \int_l \mathrm{d}x \iint_A \mathrm{d}A\left[\left(\frac{\partial x_p}{\partial q_i^e}\frac{\partial \ddot{x}_p}{\partial q_j^e} + \ddot{x}_p\frac{\partial^2 x_p}{\partial q_i^e \partial q_j^e}\right)\right. \\ & \left. + \left(\frac{\partial y_p}{\partial q_i^e}\frac{\partial \ddot{y}_p}{\partial q_j^e} + \ddot{y}_p\frac{\partial^2 y_p}{\partial q_i^e \partial q_j^e}\right) + \left(\frac{\partial z_p}{\partial q_i^e}\frac{\partial \ddot{z}_p}{\partial q_j^e} + \ddot{z}_p\frac{\partial^2 z_p}{\partial q_i^e \partial q_j^e}\right)\right],\end{aligned} \tag{15}$$

where $i,j = 1, 2, \ldots, 18$.

Eqs. (12)–(15) are obtained in implicit forms through the Gauss integral. For the beam element on the blade without a sweepback deformation, substituting $s_0 = 0$ and $T_{43} = I_{3\times 3}$ into Eqs. (12)–(15) gives the contributions of $\bar{Q}_i^{T_x}$ in linearized equation. By analogy with the aid of Eqs. (11)–(15), one can obtain the contributions of $\bar{Q}_i^{T_y}$ and $\bar{Q}_i^{T_z}$ in linearized equation.

2.5. Non-inertial force

Letting $\bar{F}_I$ represent the non-inertial force of unit mass at an arbitrary point P(x, η, ξ), the virtual work of the non-inertial force is then

$$\delta W_I = \bar{Q}_i^I \delta q_i^e, \tag{16}$$

where subscript I represents a non-inertial force

$$\bar{Q}_i^I = -\left\{ (a_h^x, a_h^y, a_h^z) + 2\left(\dot{x}_p, \dot{y}_p, \dot{z}_p\right)[w_h] + \left(x_p, y_p, z_p\right)([w_h][w_h] + [w_{ah}]) \right\} \left(\frac{\partial x_p}{\partial q_i^e}, \frac{\partial y_p}{\partial q_i^e}, \frac{\partial z_p}{\partial q_i^e} \right)^{\mathrm{T}},$$

here $[w_h]$ and $[w_{ah}]$ are transformation matrixes and are defined in Appendix E.

Using the same method as in the above section and Eq. (16), the element node force vector, gyroscopic matrix and tangential stiffness matrix respectively are found to be

$$Q_i^{I_e} = \int_l \mathrm{d}x \iint_A \bar{Q}_i^I \, \mathrm{d}A, \tag{17}$$

$$G_{ij}^{I_e} = \int_l \mathrm{d}x \iint_A \frac{\partial \bar{Q}_i^I}{\partial \dot{q}_j^e} \, \mathrm{d}A, \tag{18}$$

$$K_{ij}^{I_e} = \int_l \mathrm{d}x \iint_A \frac{\partial \bar{Q}_i^I}{\partial q_j^e} \mathrm{d}A, \tag{19}$$

where $i, j = 1, 2, \ldots, 18$.

2.6. Aerodynamic force

Based on the two-dimensional quasi-steady aerodynamic model [27], the velocity of the airflow relative to the sectional elastic center can be written as

$$\bar{V}_{ae} = \left\{ V_{ae}^x, V_{ae}^y, V_{ae}^z \right\} \left[\bar{i}_x, \bar{i}_y, \bar{i}_z \right]^{\mathrm{T}} \tag{20}$$

where $\left\{ V_{ae}^x, V_{ae}^y, V_{ae}^z \right\}$ is transformation matrix and is defined in Appendix F.

For the aerodynamic force shown in Fig. 5, one has

$$\begin{cases} U = -V_{ae}^{\eta}, \\ \dot{h} = V_{ae}^{\xi}. \end{cases} \tag{21}$$

The lift, drag and moment respectively can be expressed thus

$$L = \frac{1}{2}\rho_a a b^2 U \dot{\alpha} + \rho_a a b U \left[\dot{h} + U\alpha + \left(\frac{b}{2} - x_\alpha \right) \dot{\alpha} \right], \tag{22}$$

$$D = \rho_a b C_{d_0} U^2, \tag{23}$$

$$M = \frac{1}{2}\rho_a a b^2 U \left(\frac{b}{2} - x_\alpha \right) \dot{\alpha} + \rho_a a b U \left(\frac{b}{2} + x_\alpha \right) \left[\dot{h} + U\alpha + \left(\frac{b}{2} - x_\alpha \right) \dot{\alpha} \right] \tag{24}$$

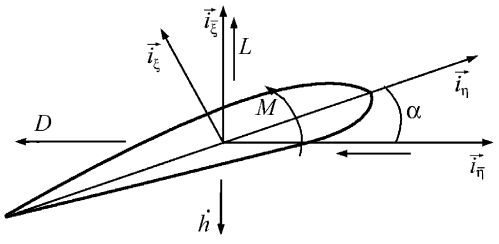

Fig. 5. Aerodynamic force.

and the virtual work done by the aerodynamic force $\bar{F}_A$ and moment $\bar{M}_A$ is

$$\delta W_A = \bar{F}_A \delta \bar{r}_p + \bar{M}_A \delta \bar{\alpha} = \bar{Q}_i^A \delta q_i^e, \tag{25}$$

where the superscript and subscript A represent aerodynamic force, and

$$\bar{Q}_i^A = \left[(0,0,L) + (0,-D,0)T_\alpha^{\mathrm{T}}\right](T_{75}T_{54}T_{43}T_{32}T_{21})\left[\frac{\partial x_{p_0}}{\partial q_i^e}, \frac{\partial y_{p_0}}{\partial q_i^e}, \frac{\partial z_{p_0}}{\partial q_i^e}\right]^{\mathrm{T}} + M\frac{\partial \alpha}{\partial q_i^e}.$$

Again, using the same method as in the above section and using Eq. (25), the element generalized force, tangential damping matrix and tangential stiffness matrix resulting from aerodynamic forces are given respectively

$$Q_i^{A_e} = \int_l \bar{Q}_i^A \mathrm{d}x, \tag{26}$$

$$C_{ij}^{A_e} = \int_l \frac{\partial \bar{Q}_i^A}{\partial \dot{q}_j^e} \mathrm{d}x, \tag{27}$$

$$K_{ij}^{A_e} = \int_l \frac{\partial \bar{Q}_i^A}{\partial q_j^e} \mathrm{d}x, \tag{28}$$

where $i,j = 1,2,\ldots,18$.

2.7. Kinetic equations of rotor blade

Due to the complexity of the rotor motion, it is more convenient for the non-inertial coordinate system to be adopted to characterize the rotor blade motion in the coupled rotor-fuselage analysis. Simultaneously, the rigid body freedoms of flap, lag and variable-pitch can be applied more realistically and effectively to describe the rotor motion. Moreover, the rotor blade can be discretized to have two generalized coordinates to quantify its elastic freedom. The equations of motion can be derived by means of the Hamilton principle:

$$\int_{t_0}^{t_n} [\delta(U - T) - \delta W]\mathrm{d}t = 0. \tag{29}$$

Substituting Eqs. (5), (10), (16) and (25) into Eq. (29), as well as preserving the independent dofs gives a nonlinear partial differential equation:

$$Q_i^T(\ddot{q}, \dot{q}, q, t) + Q_i^E(q) + Q_i^I(\dot{q}, q, t) + Q_i^A(\dot{q}, q, t) + Q_i^C(\dot{q}, q, t) = 0, \tag{30}$$

where $i = 1,2,\ldots,n$; the superscripts T, E, I, A and C represent, respectively, the contributions of kinetic energy, elastic potential energy, non-inertial force, aerodynamic force and control-operation input. The solution of Eq. (30) involves the periodic solution of the rotor aero-elastic response.

2.8. Solutions of the differential equation of motion

Using the improved quasi-linearization method [12,13], one can obtain the periodic response of the multi-dof system arising from the finite element discretization. Direct linearization of the nonlinear governing equation (30) leads to an ordinary differential equation of a periodic system in the form:

$$M_{ij}\left[q^k(t)\right]\Delta\ddot{q}_j^k + C_{ij}\left[\dot{q}^k(t), q^k(t), t\right]\Delta\dot{q}_j^k + K_{ij}\left[\dot{q}^k(t), q^k(t), t\right]\Delta q_j^k = Q_i^k(t), \tag{31}$$

where $i = 1,2,\ldots,n$, superscript k represents the kth step of iteration,

$$Q_i^k(t) = Q_i^T\left[\ddot{q}^k(t), \dot{q}^k(t), t\right] + Q_i^E\left[q^k(t)\right] + Q_i^I\left[\dot{q}^k(t), q^k(t), t\right] + Q_i^A\left[\dot{q}^k(t), q^k(t), t\right] + Q_i^C\left[\dot{q}^k(t), q^k(t), t\right].$$

The approximate solution of the $(K+1)$th step iteration is

$$q^{k+1}(t) = q^k(t) + \Delta q^k(t),$$
$$\dot{q}^{k+1}(t) = \dot{q}^k(t) + \Delta \dot{q}^k(t),$$
$$\ddot{q}^{k+1}(t) = \ddot{q}^k(t) + \Delta \ddot{q}^k(t).$$

If the required precision is satisfied, at the kth step of iteration, then the approximate solution at the $(K+1)$th step can be regarded as the nonlinear periodic solution.

3. The partition-iteration solution for the coupled rotor-fuselage analysis

The fuselage structure can be modeled as a mixed truss girder-beam model (shown in Fig. 6), and the equation of motion of the fuselage in terms of the coordinate R_0 can be established as

$$[M_F]\{\ddot{u}_F\} + [C_F]\{\dot{u}_F\} + [K_F]\{u_F\} = \{f_{HF}(t)\} + \{\bar{f}_F(t)\}. \tag{32}$$

Using Eq. (32) as an analogy, the periodic response of fuselage subjected to $\{f_{HF}(t)\}$ and $\{\bar{f}_F(t)\}$ can be solved in a coupled rotor-fuselage analysis, by means of the improved quasi-linearization method [12,13].

The complexity of the differential equation of motion of the helicopter coupled rotor-fuselage system and the difficulty of solving it requires the following new philosophy of partition-iteration to determine the dynamic response of the whole helicopter system: (1) The whole helicopter system is partitioned into several simple and independent subsystems. These subsystems should satisfy force equilibrium and deformation compatibility at the interface between each pair of subsystems. (2) The iterative method is used to find the dynamic response of each subsystem. For the coupled rotor-fuselage analysis, the whole helicopter system is partitioned into the subsystems of rotor and fuselage, and then the improved quasi-linearization method can be used to solve the solution of each subsystem. The specific procedures are as follows.

(a) The differential equations of motion of the rotor blade are established in the non-inertial coordinate system of R_1, and the non-inertial characteristics are determined from the acceleration vectors (a_h^x, a_h^y, a_h^z) and the transformation matrix $[T_{10}]$ between the coordinates R_1 and R_0. The angular velocity matrix $[w_h]$ and angular acceleration matrix $[w_{ah}]$ can be derived from $[T_{10}]$.
(b) For a given state of hub motion, the improved quasi-linearization method yields the aero-elastic response of the rotor through solution of the nonlinear dynamic equations of the rotor; the periodic force $\{f_{HF}(t)\}$ to the hub from the root of blade can be calculated.
(c) The periodic response of the fuselage is analyzed when $\{f_{HF}(t)\}$ and the foundation motion are given.
(d) The response at the junction of the rotor and fuselage is compared with the given foundation motion. If it is inconsistent, then the just-calculated periodic response should be applied as the new foundation motion of the rotor system. Procedures (a)–(c) should be repeated, until the periodic responses of the junction resulting from two consecutive iterations are approximately the same.

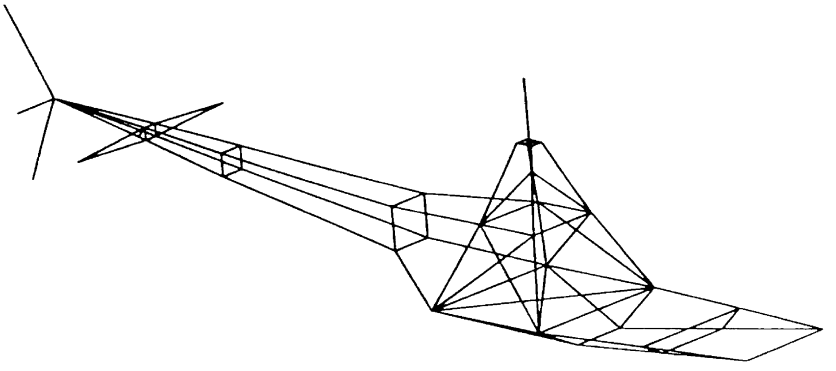

Fig. 6. Model of fuselage structure.

It is worth noting that during above solution, the coupled trim has not been used, i.e. the rotor-fuselage and trim equations have not been solved simultaneously, so the aeroelastic effects due to such interactions are neglected.

4. Verifying examples

Example 1. A rotating beam is shown in Fig. 7, and has the following parameters: density $\rho = 0.113\,\mathrm{kg/m}$, length $L = 0.508\,\mathrm{m}$, flexural rigidity $EI_y = 2.446\,\mathrm{N\,m^2}$ and $EI_z = 36.27\,\mathrm{N\,m^2}$, nondimensional rotational speed $\lambda = \Omega\sqrt{\rho l^4/EJ}$. Calculated results for different frequencies are shown in Tables 1 and 2 and are compared with results from Refs. [3,11]. Very close agreement is seen, implying that the beam element in this paper is valid and rational for dynamic analysis.

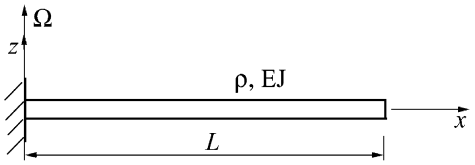

Fig. 7. Rotating beam.

Table 1
Flap frequencies (rad/s)

λ	ω					
	First-order frequency			Second-order frequency		
	Ref. [3]	Ref. [11]	This work	Ref. [3]	Ref. [11]	This work
0	63.40	63.40	63.38	397.49	397.71	396.97
2	74.64	74.66	74.58	407.96	407.96	407.42
4	100.77	100.81	100.67	437.91	437.91	437.29
6	132.80	132.87	132.68	483.74	484.10	482.96
8	167.03	167.10	166.87	541.29	541.84	540.35
10	202.08	202.26	201.95	606.98	608.06	606.02
12	237.63	237.63	237.43	678.43	680.77	677.41

Table 2
Lag frequencies (rad/s)

λ	ω		
	First-order frequency		
	Ref. [3]	Ref. [11]	This work
0	244.19	244.38	244.09
2	251.56	251.21	251.44
4	270.72	269.27	270.64
6	296.08	293.71	296.18
8	323.44	319.97	323.94
10	350.66	345.59	351.96
12	376.91	369.90	379.44

Example 2. A simple nonlinear periodic system is shown in Fig. 8. In Ref. [28], the periodic responses of this system under axial and transverse loads were discussed, having been obtained from the equivalent beam model. The parameters used in the calculation were as: flexural rigidity $EI = 3.7201 \times 10^5\,\mathrm{N\,m^2}$, density $m = 6.8244\,\mathrm{kg/m}$, length $L = 3.048\,\mathrm{m}$, elasticity ratio $K_t = 8.6123 \times 10^6\,\mathrm{N/M}$, transverse excitation load $F(t) = F_1 + F_2\sin(\Omega_1 t + \phi_t)$, axial excitation load $N_p = N_{p1} + N_{p2}\sin(\Omega_2 t + \phi_\alpha)$, here $F_1 = \phi_t = 0$, $F_2 = 1.3348 \times 10^6\,\mathrm{N}$, $\Omega_1 = 281.13\,\mathrm{rad/sec}$, $N_{p1} = \phi_\alpha = 0$, $N_{p2} = 1.5808 \times 105\,\mathrm{N}$, $\Omega_2 = 281.13\,\mathrm{rad/s}$.

In this work, a four element model of a beam with five-nodes has been used to calculate the lateral deflection at mid-span. After only 90 time steps, the calculated results are obtained (shown in Fig. 9). From Fig. 9, it is clear that complete agreement exists between them and the results of this work agree completely with that of Ref. [28].

5. Application

The vibration loads in rotor blades in a coupled rotor-fuselage system in hovering and forward flight phases are to be compared with those in system with only a single blade and those in a rotor blade system, but without a fuselage. The coupled rotor-fuselage model shown in Fig. 10 is used in the vibration load analysis.

(1) *Hovering phase*

The parameters for calculation are as follows: $\theta_0 = 0.1500\,\mathrm{rad}$, $\theta_{1c} = 0.2384 \times 10^{-2}\,\mathrm{rad}$, $\theta_{1s} = -0.3316 \times 10^{-2}\,\mathrm{rad}$, $\Omega = 40.42\,\mathrm{rad/s}$, $V_F = 0.00\,\mathrm{km/h}$, $\alpha_F = 0.00\,\mathrm{rad}$. Figs. 11(a) and (b) show the flap flexibility and acceleration at the peak point of the rotor blade as they vary with azimuth angle. The lag flexibility and acceleration at the peak point of the rotor blade, varying with azimuth angle, are shown in Figs. 12(a) and (b). The flap flexibility and acceleration at the rotor blade midpoint, varying with azimuth

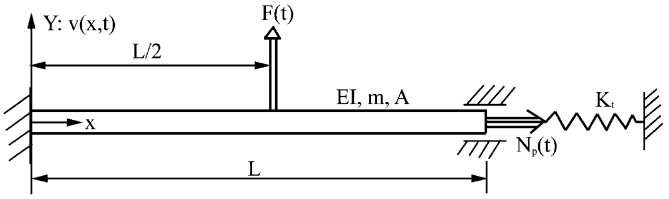

Fig. 8. Periodic system.

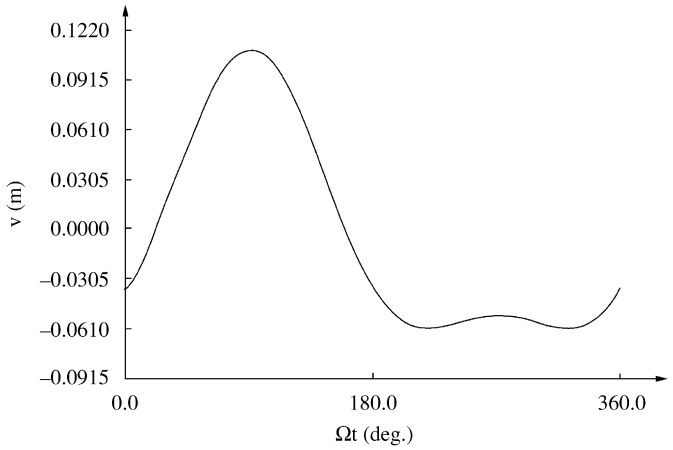

Fig. 9. Lateral deflection at midspan.

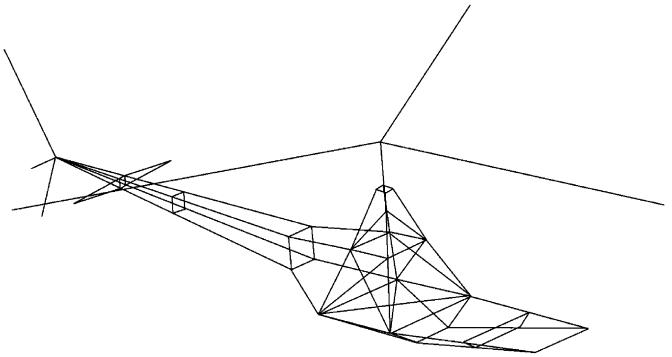

Fig. 10. Coupled rotor-fuselage model.

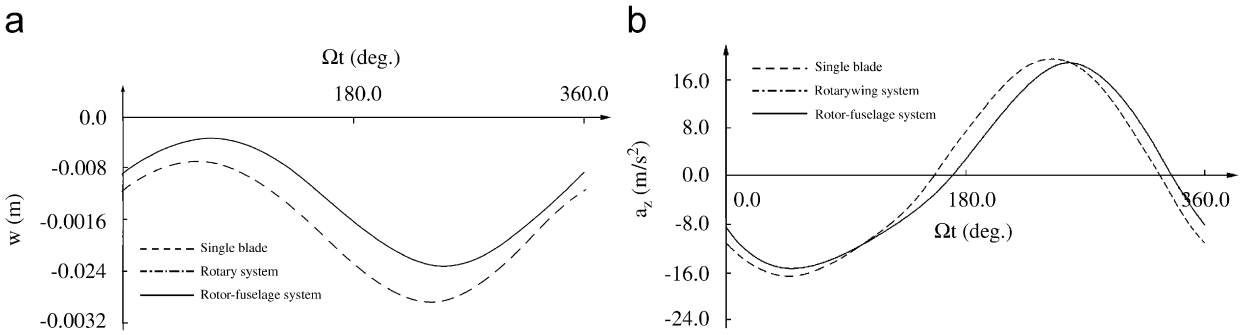

Fig. 11. Flap (a) flexure and (b) acceleration at the peak point of rotor blade varying with azimuth angle.

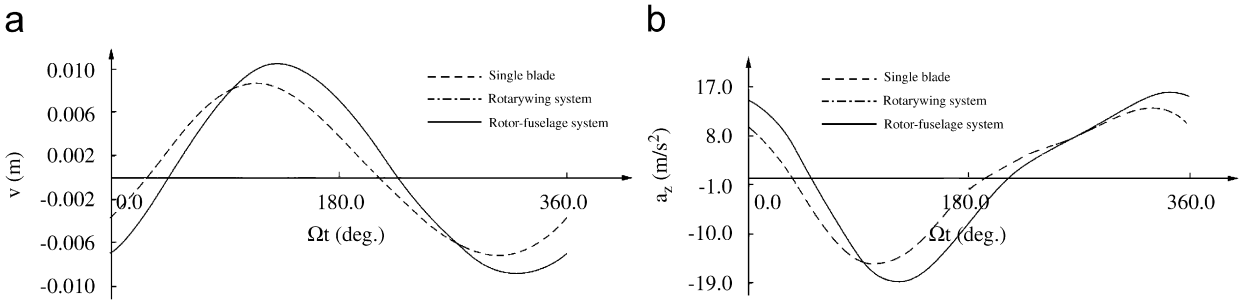

Fig. 12. Lag (a) flexure and (b) acceleration at the peak point of rotor blade varying with azimuth angle.

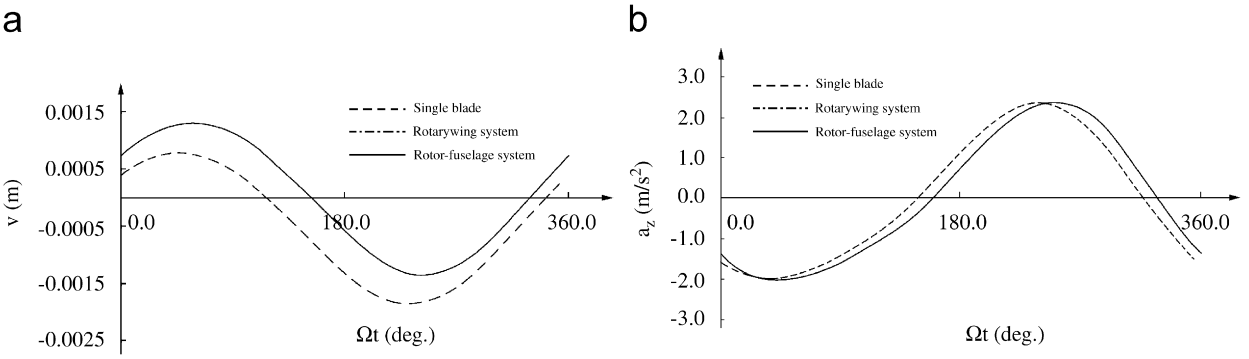

Fig. 13. Flap (a) flexure and (b) acceleration at the midpoint of rotor blade varying with azimuth angle.

angle, are calculated and shown in Figs. 13(a) and (b). The lag flexibility and acceleration at the rotor blade midpoint, varying with azimuth angle, are shown in Figs. 14(a) and (b). The flap, lag and variable pitch angles, varying with azimuth angle, are shown respectively in Figs. 15(a)–(c). The periodic forces in the X and Y directions, acting on the hub in the coordinate of R_0, varying with azimuth angle, are shown in Figs. 16(a) and (b). The periodic moments in the X and Y directions, acting on the hub in the coordinate of R_0, varying with azimuth angle, are shown in Figs. 17(a) and (b).

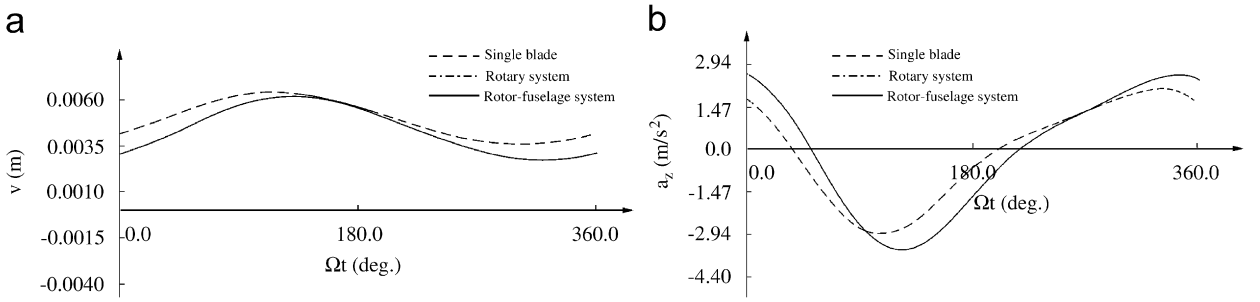

Fig. 14. Lag (a) flexure and (b) acceleration at the midpoint of rotor blade varying with azimuth angle.

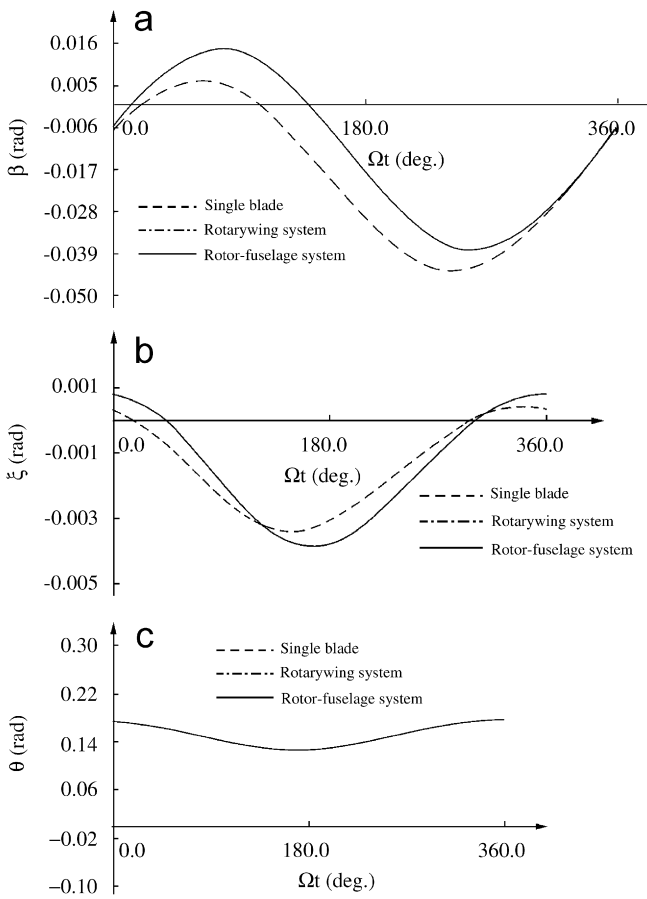

Fig. 15. Flap (a) angle varying with azimuth angle, (b) lag angle varying with azimuth angle, and (c) pitch angle varying with azimuth angle.

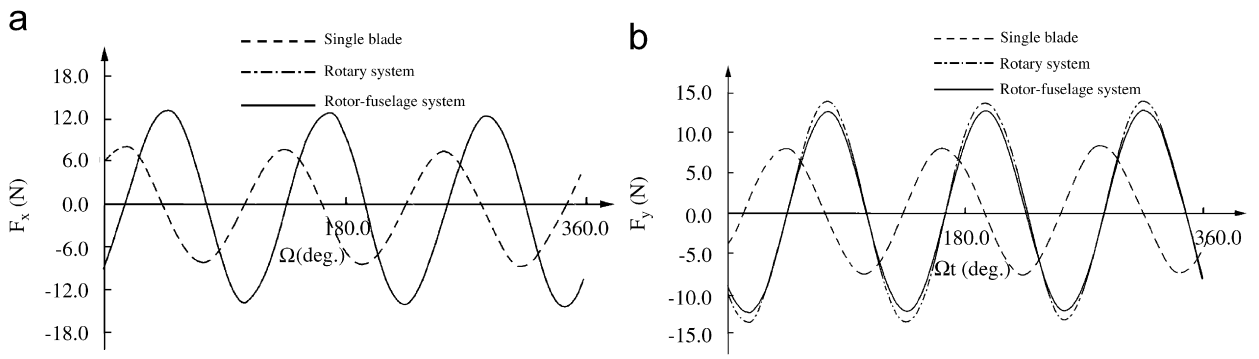

Fig. 16. Periodic forces in (a) X and (b) Y directions, acting on the hub in the coordinate of R_0, varying with azimuth angle.

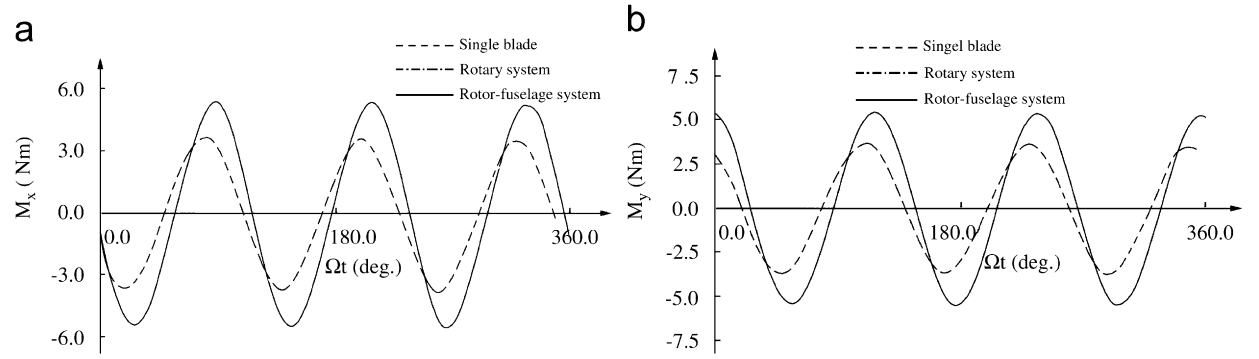

Fig. 17. Periodic moments in (a) X and (b) Y directions, acting on the hub in the coordinate of R_0, varying with azimuth angle.

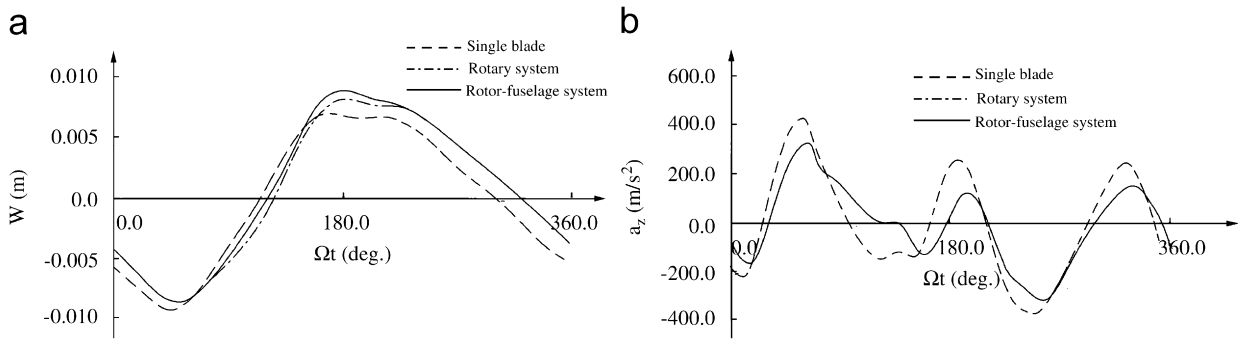

Fig. 18. Flap (a) flexure and (b) acceleration at the peak point of rotor blade varying with azimuth angle.

(2) *Forward flight phase*

The parameters for calculation are as follows: $\theta_0 = 0.1367\,\text{rad}$, $\theta_{1c} = -0.9680 \times 10^{-1}\,\text{rad}$, $\theta_{1s} = 0.13326 \times 10^{-1}\,\text{rad}$, $\Omega = 40.42\,\text{rad/s}$, $V_F = 197.25\,\text{km/h}$, $\alpha_F = 0.169\,\text{rad}$. The flap flexibility and acceleration at the peak point of the rotor blade, varying with azimuth angle, are calculated and shown in Figs. 18(a) and (b). The lag flexibility and acceleration at the peak point of the rotor blade, varying with azimuth angle, are shown in Figs. 19(a) and (b). The flap flexibility and acceleration at the rotor blade midpoint, varying with azimuth angle, are calculated and shown in Figs. 20(a) and (b). The lag flexibility and acceleration at the rotor blade midpoint, varying with azimuth angle, are shown in Figs. 21(a) and (b). The flap, lag and variable pitch

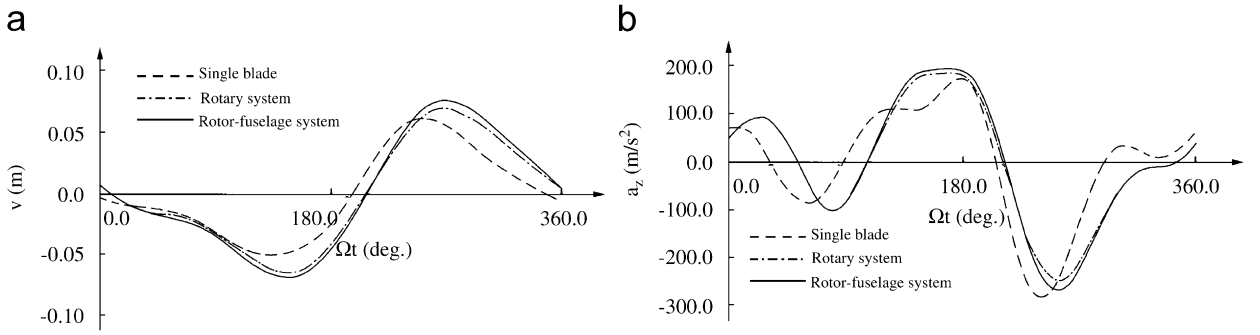

Fig. 19. Lag (a) flexure and (b) acceleration at the peak point of rotor blade varying with azimuth angle.

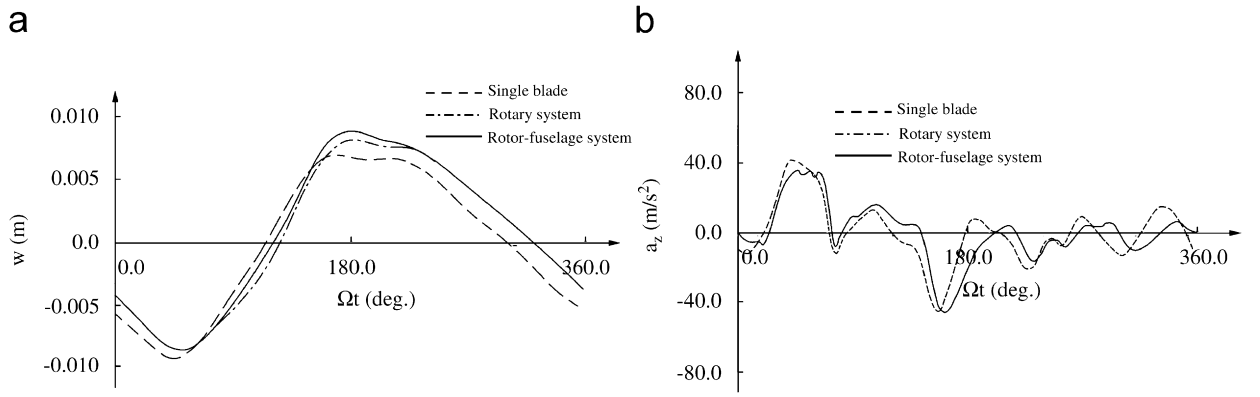

Fig. 20. Flap (a) flexure and (b) acceleration at the midpoint of rotor blade varying with azimuth angle.

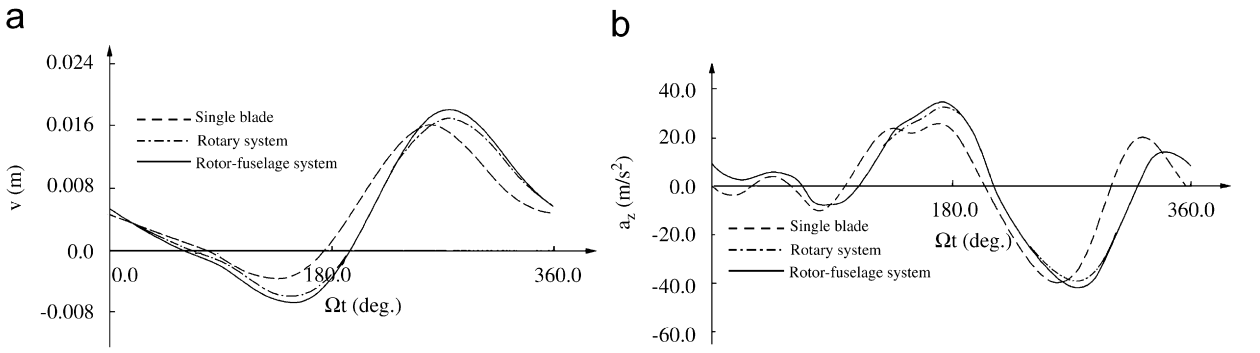

Fig. 21. Lag (a) flexure and (b) acceleration at the midpoint of rotor blade varying with azimuth angle.

angles, varying with azimuth angle, are shown, respectively, in Figs. 22(a)–(c). The periodic forces in the X and Y directions, acting on the hub in the coordinate of R_0, varying with azimuth angle, are shown in Figs. 23(a) and (b). The periodic moments in the X and Y directions, acting on the hub in the coordinate of R_0, varying with azimuth angle, are shown in Figs. 24(a) and (b).

From Figs. 11 to 24, it is apparent that the maximum relative deviation between the vibration loads of a rotor blade in a coupled rotor-fuselage system and those in a rotor blade system without fuselage is less than 10%. The calculated vibration loads in a rotor blade in a coupled rotor-fuselage system are very close to those in a rotor blade system without fuselage. In particular the calculated results for the hovering phase are nearly coincident. The efforts in this paper have a good agreement with those in literature [24].

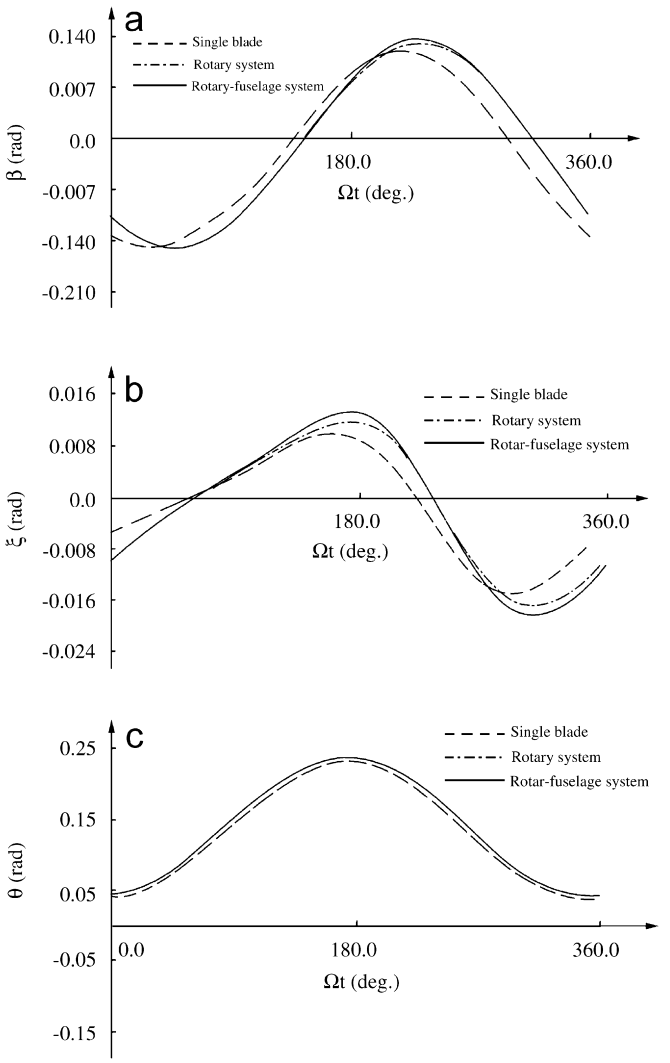

Fig. 22. Flap (a) angle varying with azimuth angle, (b) Lag angle ζ (rad) varying with azimuth angle, (c) Pitch angle θ (rad) varying with azimuth angle.

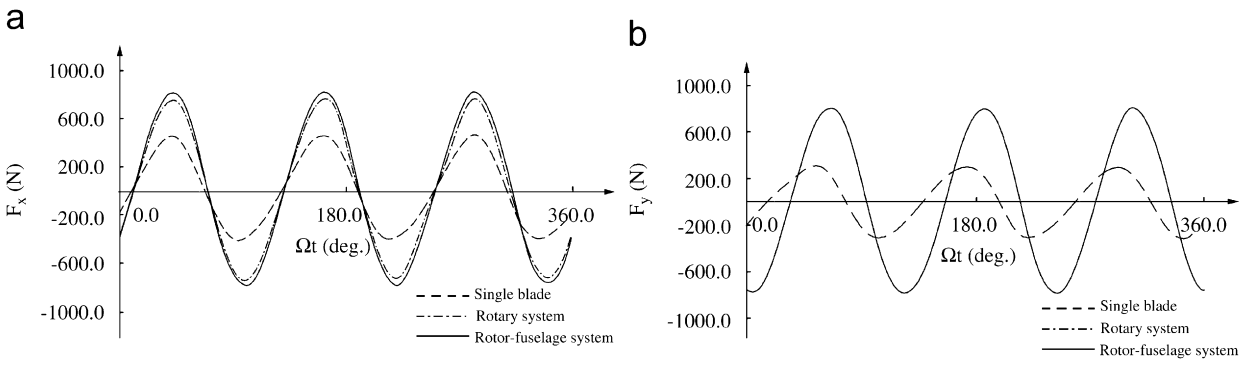

Fig. 23. Periodic forces in (a) X and (b) Y directions, acting on the hub in the coordinate of R_0, varying with azimuth angle.

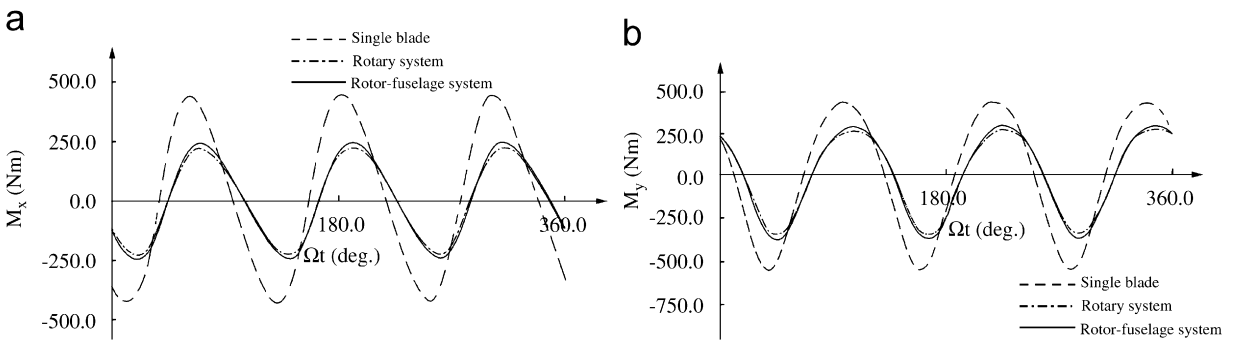

Fig. 24. Periodic moments in (a) X and (b) Y directions, acting on the hub in the coordinate of R_0, varying with azimuth angle.

However, there exist obvious differences between the calculated vibration loads in the coupled rotor-fuselage system and those in the system with only a single rotor blade. This implies the vibration loads of the rotor blade are more heavily influenced by the elastic behavior of the shafting bearing, than by the elastic behavior of the fuselage.

6. Closure

The focus of this paper has been to present an integral and new nonlinear coupled helicopter rotor-fuselage aeroelasticity model with many dof and a novel partition-iteration method to solve the structural response and the vibration loads of rotor blades. The applicability of the new model and solution method has been shown for a helicopter coupled rotor-fuselage system for estimating the vibration load in rotor blade.

Acknowledgment

This project was supported by the National Natural Science Foundation, the National Defence Foundation and Aeronautics Science Foundation in People's Republic of China.

We wish to thank Professor Denys J. Mead of the Institute of Sound and Vibration Research, University of Southampton, United Kingdom, for his help in improving the English of this paper.

Appendix A. Shape function

$$
\begin{aligned}
u(s) &= N_{u_1}(s)u_1 + N_{u_3}(s)u_3 + N_{u_4}(s)u_4 + N_{u_2}(s)u_2,\\
v(s) &= N_{v_1}(s)v_1 + N_{v_1'}(s)v_1' + N_{v_2}(s)v_2 + N_{v_2'}(s)v_2',\\
w(s) &= N_{w_1}(s)w_1 + N_{w_1'}(s)w_1' + N_{w_2}(s)w_2 + N_{w_2'}(s)w_2',\\
\phi(s) &= N_{\phi_1}(s)\phi_1 + N_{\phi_3}(s)\phi_3 + N_{\phi_2}(s)\phi_2,
\end{aligned}
$$

where

$$
\begin{aligned}
N_{u_1}(s) &= (1-s)[-10+9(s^2+1)]/16, \quad N_{u_2}(s) = (1-s)[-10+9(s^2+1)]/16,\\
N_{u_3} &= 9(1-s^2)(1-3s)/16, \quad N_{u_4} = 9(1-s^2)(1-3s)/16,
\end{aligned}
$$

$$
\begin{aligned}
N_{v_1}(s) &= (1-s)^2(2+s)/4, \quad N_{v_1'}(s) = l(1-s)^2(s+1)/8,\\
N_{v_2}(s) &= (1-s)^2(2-s)/4, \quad N_{v_2'}(s) = l(1+s)^2(s-1)/8,
\end{aligned}
$$

$$N_{w_1}(s)=N_{v_1}(s),\quad N_{w_1'}(s)=N_{v_1'}(s),\quad N_{w_2}(s)=N_{v_2}(s),\quad N_{w_2'}(s)=N_{v_2'}(s)$$
$$N_{\phi_1}(s)=s(s-1)/2,\quad N_{\phi_3}(s)=(1-s)(1+s),\quad N_{\phi_2}(s)=s(s+1)/2$$

Appendix B. Section properties

$$\bar{A}=\overline{A}_1+\overline{A}_2+\overline{A}_3,\quad \overline{A}_1=\begin{bmatrix} D & & \\ & G & \\ & & G\end{bmatrix},\quad \overline{A}_2=D\theta'\begin{bmatrix} 0 & \xi & -\eta\\ \xi & 0 & 0\\ -\eta & 0 & 0\end{bmatrix},$$
$$\overline{A}_3=\begin{bmatrix} 0 & 0 & 0\\ 0 & \xi^2 & -\xi\eta\\ 0 & -\xi\eta & \eta^2\end{bmatrix}\cdot D\theta'^2,\quad D=\frac{E(1-\mu)}{(1-\mu)(1-2\mu)},$$

$$\overline{V}_x=DA\left[u'+\frac{1}{2}\left(v'^2+w'^2\right)\right]-e_\eta[v''\cos(\theta+\phi)+w''\sin(\theta+\phi)]+e_\xi[v''\sin(\theta+\phi)+w''\cos(\theta+\phi)]$$
$$\overline{M}_y=DAe_\xi\left[u'+\frac{1}{2}\left(v'^2+w'^2\right)\right]+DJ_y[v''\sin(\theta+\phi)-w''\cos(\theta+\phi)]$$
$$\overline{M}_z=-DAe_\eta\left[u'+\frac{1}{2}\left(v'^2+w'^2\right)\right]+DJ_z[v''\cos(\theta+\phi)+w''\sin(\theta+\phi)]$$
$$A=\iint_A \mathrm{d}\eta\,\mathrm{d}\xi,\quad e_\eta=\iint_A \eta\,\mathrm{d}\eta\,\mathrm{d}\xi,\quad e_\xi=\iint_A \xi\,\mathrm{d}\eta\,\mathrm{d}\xi,$$
$$J_y=\iint_A \xi^2\,\mathrm{d}\eta\,\mathrm{d}\xi,\quad J_z=\iint_A \eta^2\,\mathrm{d}\eta\,\mathrm{d}\xi,\quad J=\iint_A (\xi^2+\eta^2)\mathrm{d}\eta\,\mathrm{d}\xi$$

where E is elastic modulus and μ is the Poisson ratio.

Appendix C. Coordinate transformation matrixes

$$T_{21}=\begin{bmatrix}\cos(\beta_0+\beta) & 0 & \sin(\beta_0+\beta)\\ 0 & 1 & 0\\ -\sin(\beta_0+\beta) & 0 & \cos(\beta_0+\beta)\end{bmatrix},\quad T_{32}=\begin{bmatrix}\cos\xi & -\sin\xi & 0\\ \sin\xi & \cos\xi & 0\\ 0 & 0 & 1\end{bmatrix},$$
$$T_{43}=\begin{bmatrix}1 & 0 & 0\\ 0 & \cos\theta_p & \sin\theta_p\\ 0 & -\sin\theta_p & \cos\theta_p\end{bmatrix},\quad T_{54}=\begin{bmatrix}\cos\xi_0 & \sin\xi_0 & 0\\ -\sin\xi_0 & \cos\xi_0 & 0\\ 0 & 0 & 1\end{bmatrix},$$
$$T_{75}=\begin{bmatrix}1 & v' & w'\\ -w'\sin(\theta+\phi)-v'\cos(\theta+\phi) & \cos(\theta+\phi) & \sin(\theta+\phi)\\ -w'\cos(\theta+\phi)+v'\sin(\theta+\phi) & -\sin(\theta+\phi)-v'w'\cos(\theta+\phi) & \cos(\theta+\phi)\end{bmatrix}.$$

Appendix D. Kinetic and strain energy terms

$$\bar{Q}_i^{T_x} = \frac{\mathrm{d}}{\mathrm{d}t}\left(\dot{x}_p \frac{\partial \dot{x}_p}{\partial \dot{q}_i^e}\right) - \dot{x}_p \frac{\partial \dot{x}_p}{\partial \dot{q}_i^e} = \ddot{x}_p \frac{\partial x_p}{\partial q_i^e} \quad (i = 1, 2, \ldots, 18),$$

$$\bar{Q}_i^{T_y} = \ddot{y}_p \frac{\partial y_p}{\partial q_i^e} \quad (i = 1, 2, \ldots, 18),$$

$$\bar{Q}_i^{T_z} = \ddot{z}_p \frac{\partial z_p}{\partial q_i^e} \quad (i = 1, 2, \ldots, 18),$$

where q_{16}^e, q_{17}^e and q_{18}^e correspond respectively to flap, lag and variable-pitch, or β, ζ and θ_p.

Appendix E. Transformation matrixes

$$[w_h] = \begin{bmatrix} 0 & w_h^z & -w_h^y \\ -w_h^z & 0 & w_h^x \\ w_h^y & -w_h^x & 0 \end{bmatrix}, \quad [w_{ah}] = \begin{bmatrix} 0 & w_{ah}^z & -w_{ah}^y \\ -w_{ah}^z & 0 & w_{ah}^x \\ w_{ah}^y & -w_{ah}^x & 0 \end{bmatrix}.$$

Appendix F. Transformation matrixes

$$\left(V_{ae}^x, V_{ae}^y, V_{ae}^z\right) = \left\{\left(V_{ae}^{x_0}, V_{ae}^{y_0}, V_{ae}^{z_0}\right) - \left(x_{p_0}, y_{p_0}, z_{p_0}\right)[w_h] - \dot{q}_k^e \left(\frac{\partial x_{p_0}}{\partial q_k^e}, \frac{\partial y_{p_0}}{\partial q_k^e}, \frac{\partial z_{p_0}}{\partial q_k^e}\right)\right\} (T_{75} T_{54} T_{43} T_{32} T_{21})^{\mathrm{T}} T_{\alpha}^{\mathrm{T}},$$

$$\left(V_{ae}^{x_0}, V_{ae}^{y_0}, V_{ae}^{z_0}\right) = (V_F \cos\alpha_F, 0, -V_F \sin\alpha_F)[T_{10}] + (0, 0, V_i),$$

$$\alpha = \theta_p + \theta + \phi,$$

$$[T_\alpha] = \begin{bmatrix} 1 & 0 & 0 \\ 0 & \cos(\theta_p + \theta + \phi) & \sin(\theta_p + \theta + \phi) \\ 0 & -\sin(\theta_p + \theta + \phi) & \cos(\theta_p + \theta + \phi) \end{bmatrix}.$$

References

[1] R. Heffernan, Effect of helicopter blade dynamics on blade aerodynamic and structural loads, *Journal of the American Helicopter Society* 33 (3) (1988) 30–41.

[2] M.S. Torok, I. Chopra, Rotor loads prediction utilizing a coupled aeroelastic analysis with refined aerodynamic modeling, *Journal of the American Helicopter Society* 36 (1) (1991) 58–67.

[3] D.H. Hodges, M.J. Rutkowski, Free vibration analysis of rotating beams by a variable-order finite element method, *AIAA Journal* 19 (11) (1981) 1459–1466.

[4] S. Rao, R. Gupta, Finite element vibration analysis of rotating Timoshenko beams, *Journal of Sound and Vibration* 242 (2001) 103–124.

[5] S. Lin, K. Hsio, Vibration analysis of a rotating Timoshenko beam, *Journal of Sound and Vibration* 240 (2001) 303–322.

[6] D. Diker, Vibration control of a rotating Euler-Bernoulli beam, *Journal of Sound and Vibration* 232 (2000) 541–551.

[7] J. Chung, H. Yoo, Dynamic analysis of a rotating cantilever beam by using the finite element method, *Journal of Sound and Vibration* 249 (2002) 147–164.

[8] P.P. Friedmann, F. Straub, Application of the finite element method to rotary-wing aeroelasticity, *Journal of American Helicopter Society* 25 (1980) 36–44.

[9] N.T. Sivaneri, I. Chopra, Dynamic stability of a rotor blade using finite element analysis, *AIAA Journal* 20 (1982) 716–723.

[10] D. Thakkar, R. Ganguli, Dynamic response of rotating beams with piezoceramic actuation, *Journal of Sound and Vibration* 270 (4–5) (2004) 729–753.

[11] O.A. Bauchau, C.H. Hong, Nonlinear response and stability analysis of beams using finite elements in time, *AIAA Journal* 26 (9) (1988) 1135–1142.

[12] R. Celi, P.P. Friedmann, Rotor blade aeroelasticity in forward flight with an implicit aerodynamic formulation, *AIAA Journal* 26 (12) (1988) 1425–1433.
[13] R. Celi, Helicopter rotor blade aeroelasticity in forward flight with an implicit structural formulation, *AIAA Journal* 30 (9) (1992) 2274–2282.
[14] M.R.M. Crespo Da Silva, A comprehensive analysis of the dynamics of a helicopter rotor blade, *International Journal of Solids and Structures* 35 (7–8) (1998) 619–635.
[15] R. Ganguli, Optimum design of a helicopter rotor for low vibration using aeroelastic analysis and response surface methods, *Journal of Sound and Vibration* 258 (2) (2002) 327–344.
[16] A. El-Sinawi, M.N. Hamdan, Optimal vibration estimation of a non-linear flexible beam mounted on a rotating compliant hub, *Journal of Sound and Vibration* 259 (4) (2003) 857–872.
[17] S.R. Viswamurthy, R. Ganguli, An optimization approach to vibration reduction in helicopter rotors with multiple active trailing edge flaps, *Aerospace Science and Technology* 8 (3) (2004) 185–194.
[18] I. Papavassiliou, P.P. Friedmann, C. Venkatesan, Coupled rotor-fuselage vibration reduction using open-loop blade pitch control, *Mathematical and Computer Modelling* 18 (3–4) (1993) 131–156.
[19] H. Yeo, I. Chopra, Coupled rotor/fuselage vibration analysis for teetering rotor and test data comparison, *Journal of Aircraft* 38 (1) (2001) 111–121.
[20] M.J. Rutkowski, Assessment of rotor-fuselage coupling on vibration predictions using a simple finite element model, *Journal of the American Helicopter Society* 28 (3) (1983) 20–25.
[21] T.K. Hsu, D.A. Peters, Coupled rotor/airframe vibration analysis by a combined harmonic-balance, impedance-matching method, *Journal of the American Helicopter Society* 27 (1) (1982) 25–34.
[22] D.L. Kunz, A nonlinear response analysis and solution method for rotorcraft vibration, *Journal of the American Helicopter Society* 28 (1) (1983) 56–62.
[23] W. Stephens, D.A. Peter, Rotor-body coupled revisited, *Journal of the American Helicopter Society* 32 (1987) 68–72.
[24] R.C. Cribbs, P.P. Friedmann, T. Chiu, Coupled helicopter rotor/flexible fuselage aeroelastic model for control of structural response, *AIAA Journal* 38 (10) (2000) 1777–1788.
[25] O. Bauchau, J. Rodriguez, S.Y. Chen, Coupled rotor-fuselage analysis with finite motions using component mode synthesis, *Journal of the American Helicopter Society* 50 (2) (2004) 201–211.
[26] Y.Z. Feng, *Introduction of Continuum Mechanics*, Science Press, Beijing, 1984 (in Chinese).
[27] Z.Q. Zhu, *Applied Computational Fluent Mechanics*, Beihang University Press, Beijing, 1998 (in Chinese).
[28] P.P. Friedmann, Numerical methods for the treatment of periodic systems with applications to structural dynamics and helicopter rotor dynamics, *Computers and Structures* 35 (4) (1990) 329–347.